Dossier

This paper is a part of the hereunder thematic dossier published in OGST Journal, Vol. 70, No. 1, pp. 3-211 and available online here

Cet article fait partie du dossier thématique ci-dessous publié dans la revue OGST, Vol. 70, n°1, pp. 3-211 et téléchargeable ici

DOSSIER Edited by/Sous la direction de : **B. Leduc et P. Tona**

IFP Energies nouvelles International Conference / Les Rencontres Scientifiques d'IFP Energies nouvelles
E-COSM'12 — IFAC Workshop on Engine and Powertrain Control, Simulation and Modeling
E-COSM'12 — Séminaire de l'IFAC sur le contrôle, la simulation et la modélisation des moteurs et groupes moto-propulseurs

Oil & Gas Science and Technology – Rev. IFP Energies nouvelles, Vol. 70 (2015), No. 1, pp. 3-211

IFP Energies nouvelles

Oil & Gas Science and Technology – Rev. IFP Energies nouvelles, Vol. 70 (2015), No. 1, pp. 125-141

DOI: 10.2516/ogst/2013215

OPEN ACCESS

IFP Energies nouvelles International Conference
Rencontres Scientifiques d'IFP Energies nouvelles

E-COSM'12 - IFAC Workshop on Engine and Powertrain Control, Simulation and Modeling
E-COSM'12 - Séminaire de l'IFAC sur le contrôle, la simulation et la modélisation des moteurs et groupes moto-propulseurs

Energy Management Strategies for Diesel Hybrid Electric Vehicle

Olivier Grondin*, Laurent Thibault and Carole Quérel

IFP Energies nouvelles, 1-4 avenue de Bois-Préau, 92852 Rueil-Malmaison Cedex - France
e-mail: olivier.grondin@ifpen.fr - laurent.thibault@ifpen.fr - carole.querel@ifpen.fr

* Corresponding author

Abstract — *This paper focuses on hybrid energy management for a Diesel Hybrid Electric Vehicle (HEV) with a parallel architecture. The proposed strategy focuses on the reduction of Nitric Oxides (NO_x) emissions that represents a key issue to meet Diesel emissions standards. The strategy is split in two separated functions aiming at limiting the NO_x in steady-state and transient operating conditions. The first functions, control the torque split between the engine and the electric motor. This energy management is based on the Equivalent Consumption Minimization Strategy (ECMS) where an additional degree of freedom is introduced to tune the optimization trade-offs from the pure fuel economy case to the pure NO_x limitation case. The second function adapts the torque split ratio between the motor and the engine, initially computed from the optimal control strategy during transient operations where NO_x are produced. The engine torque correction relies on mean value models for the EGR system dynamics and for the NO_x formation. This paper applies a methodology based on Software in the Loop (SiL) and Hardware in the Loop (HiL) simulations in order to understand the system performance according to the powertrain configurations and also to tune the proposed energy management strategy. The simulation results are confirmed by experiments performed on Hybrid-Hardware in the Loop (Hy-HiL) test bench. This work shows the potential of using the hybrid architecture to limit NO_x emissions by choosing the best operating point and by limiting the engine dynamics. The NO_x reduction has limited impact on fuel consumption.*

Résumé — **Lois de gestion de l'energie pour le véhicule hybride Diesel** — Cet article présente une stratégie de gestion de l'énergie pour un véhicule hybride parallèle muni d'une motorisation Diesel. Cette stratégie est consacrée à la réduction des émissions d'oxydes d'azote (NO_x) dont la dépollution constitue une problématique majeure pour l'homologation des véhicules Diesel. La stratégie comporte deux fonctions distinctes visant à limiter les émissions de NO_x en régime stabilisé et en régime transitoire. La première fonction agit sur la répartition de couple entre le moteur thermique et la machine électrique. L'approche ECMS (*Equivalent Consumption Minimization Strategy*, ou stratégie de minimisation de la consommation équivalente) est utilisée pour gérer la réparation de couple et dans notre cas elle intègre dans la fonction coût un compromis entre la consommation et les émissions de NO_x. La seconde fonction corrige la répartition de couple issue de l'ECMS mais uniquement en régime transitoire et afin de réduire les pics d'émissions de NO_x. L'adaptation de la répartition de couple repose sur des modèles moyens du système EGR et de la formation des NO_x. Cet article présente le principe de ces stratégies et leur comportement est analysé grâce à un simulateur représentatif des émissions polluantes. Ces résultats sont complétés par des essais expérimentaux sur un banc moteur HiL

(*Hardware in the Loop*). Ce travail montre qu'il est possible de limiter les émissions de NO_x par le biais de l'hybridation en adaptant le choix du point de fonctionnement du moteur et en réduisant les sollicitations transitoires pendant lesquelles les NO_x sont produits. La réduction des émissions de NO_x n'est pas obtenue au détriment de la consommation.

NOMENCLATURE

PARAMETERS & VARIABLES

α_i	NO_x model parameters (-)
F_1	Intake burned gas ratio (-)
β_d	EGR model time delay (s.rpm)
β_f	EGR model time constant (s.rpm)
k_{fc/NO_x}	Emissions weighting factor (-)
N_e	Engine speed (rpm)
R_1	Front axle ratio (-)
R_{gb}	Gear Box ratio (-)
SOC	Battery state of charge (%)
Θ	Temperature (K)
t	Time (s)
T	Torque (Nm)
u	Control input (Nm)
ξ	NO_x reduction factor (%)

SUBSCRIPTS & SUPERSCRIPTS

b	Burned gas
cyl	Cylinder
eng	Engine
est	Estimated
f	Feasible
mot	Motor
pwt	Powertrain
ss	Steady-state
sp	Setpoint
t	Trajectory

ACRONYMS

BGR	Burned Gas Ratio
DPF	Diesel Particulate Filter
ECMS	Equivalent Consumption Minimization Strategy
EGR	Exhaust Gas Recirculation
EM	Electric Machine
EMS	Energy Management Strategy
FC	Fuel Consumption
FTP	Federal Transient Procedure
GB	Gear Box
HEV	Hybrid Electric Vehicle
HP	High Pressure (EGR)
LP	Low Pressure (EGR)
MVM	Mean Value Model
NEDC	New European Drive Cycle
NO_x	Nitrogen oxides
S&S	Stop & Start
SOC	State of Charge
SSG	Separated Starter-Generator
SSP	Steady-State Part
TP	Transient Part
VVA	Variable Valve Actuation
WLTP	Worldwide harmonized Light-duty Transient Procedure

INTRODUCTION

In a context of increasing demand for cleaner vehicles, hybrid electric vehicles are recognized as an effective way to reduce fuel consumption and emissions. The most common hybrid powertrains usually combine a gasoline engine with an electric motor with different architectures and several degrees of hybridization. The pollutant emissions of the gasoline engine are treated by the three-way catalytic converter. For the gasoline hybrid vehicle, the energy efficiency improvement is the main objective. Thus, the energy supervisor improves the fuel economy rather than the emissions in warm conditions while the thermal management is the main issue in cold conditions [1]. If we consider hybrid powertrains with a Diesel engine, the Nitrogen Oxide (NO_x) emissions must be considered because the operating regions of maximum efficiency and minimum NO_x emissions are generally not the same. For this purpose, the energy management strategy must be adapted to maximize the use of the engine within its low NO_x emissions operating points.

This control issue was studied in the literature mainly in simulation. Early work from Johnson *et al.* [2] deals with heuristic supervision strategies for a Diesel HEV. The latter takes into account fuel consumption weighted with the four main pollutants (NO_x, PM,

HC, CO). Other heuristic strategies are proposed in [3]. On the other hand, model-based techniques have already been proposed by Lin *et al.* [4] (ECMS) and Musardo *et al.* [5, 6] (dynamic programming). More recently, Dextreil and Kolmanovsky [7] propose an energy management controller based on the application of game theory. The simulation and experimental results from these papers indicate that a significant NO_x reduction is possible at the price of a slight drop in fuel consumption. These papers confirm the feasibility of integrating emission constraints into heuristic or model-based supervision strategies.

These solutions can be applied for Euro 6 engines but new constraints will arise from the transient nature of the upcoming Worldwide harmonized Light vehicles Test Procedures (WLTP). Indeed if we consider only the current European driving cycle, the transient part of the total NO_x emissions can clearly be neglected. But these transient emissions are actually significant with the new driving cycle which is more representative of real world conditions. In this context, the current strategies applying optimal control based on static maps are not sufficient and NO_x transient emissions should be taken into account.

The goal of this paper is to propose a global energy management strategy for Diesel HEV taking into account both static and transient NO_x emissions in addition to the fuel consumption objective. In our approach, the steady-state and transient parts are treated separately as described in Figure 1. The steady state optimal torque splits are found using the optimal control theory. The engine torque $T^{sp}_{eng,ss}$ and motor torque $T^{sp}_{mot,ss}$ setpoints are computed from an ECMS-based strategy including the steady-state NO_x emission maps into the cost function. The second function consists of a model-based strategy that adapts the static torque split during the transient phases where NO_x peaks can occur. This leads to a computation of two trajectories for the engine torque ($T^{sp}_{eng,t}$) and the motor torque ($T^{sp}_{mot,t}$).

The paper is organized as follows: the vehicle architecture is presented in the first part of the paper (*Sect. 1.1*) with the modeling aspects (Sect. 1.2) and the presentation of the EMS based on the equivalent consumption minimization strategy (Sect. 1.3). The steady-state strategy performances are analysed in simulation and some experimental results are shown in Section 1.4. In the second part of the paper, we highlight the transient NO_x emissions problem in Diesel engines (Sect. 2.1). The principle of the engine torque setpoint control and the NO_x trajectory definition are detailed in Section 2.2. The strategy is validated in simulation and the results are discussed in Section 2.3. Finally, this paper ends up with conclusions.

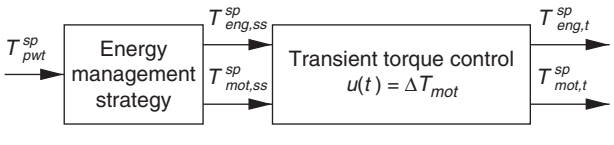

Figure 1

Static and dynamic torque split strategy based on a transient torque controller cascaded with a ECMS-based controller.

1 ADAPTATION OF THE EMS FOR DIESEL ENGINE: MINIMIZATION OF NO_X ALONG WITH FUEL CONSUMPTION

1.1 System Description

In this paper, we consider the vehicle architecture depicted in Figure 2. This is a parallel hybrid architecture that uses a Separated Starter Generator (SSG) in the pre-transmission side (only allowed to start the engine) and the post-transmission Electric Machine (EM) allows for power assist, full electric drive, regenerative braking and battery recharge. More details about the hybrid parallel vehicle can be found in [8]. The Diesel engine is a 1.6 liter, four-cylinder, direct-injection engine with a maximum power of 50 kW and a maximum torque of 150 Nm. The engine uses high EGR rate to operate under low temperature combustion mode such that the engine NO_x emissions are close to the Euro 6 emission standard without dedicated post-treatment. To supply the cylinder with EGR, the engine has a Low Pressure (LP) EGR loop. The LP EGR circuit takes

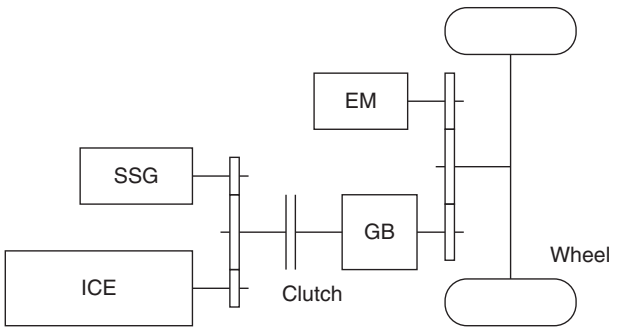

Figure 2

Parallel hybrid-electric propulsion system under consideration.

TABLE 1
Parameters of the hybrid powertrain considered in this paper: vehicle mass, electric motor power and battery energy

Vehicle mass (kg)	EM power (kW)	Battery energy (wh)
1 470	8	280
1 580	14	520
1 630	20	720

the exhaust gases downstream after the treatment system – composed of a Diesel Oxidation Catalyst (DOC) and a Diesel Particulate Filter (DPF) – to upstream the compressor. In this paper, we consider only the LP EGR operations. In this configuration, the system has a slower burned gas settling time compared to the HP EGR mode. The engine transients are then more drastic according to the NO_x emission peaks since they are mostly caused by EGR time lag. This is a fancy case study to develop and validate a transient NO_x limitation strategy using the power assist from the electric machine (Sect. 2). In this work, we perform a parametric study of the electric machines power. We adopt a basic rule to adapt the battery size in order to keep the battery energy to motor power ratio constant and close to 35 Wh/kW. This value is chosen according to the reference hybrid system where the electric motor has a rated power of 42 kW and the battery an energy of 1.5 kWh [9]. The vehicle mass is also adapted to account for the electric machine and battery size. This leads to the configuration detailed in Table 1.

1.2 System Modeling

The aim of this section is to introduce the mathematical model of the parallel hybrid powertrain shown in Figure 2. The model has a backward causality and it is of the quasi-static type. All the dynamics except for the vehicle longitudinal dynamics and the battery accumulator dynamics are neglected. These models equations are accepted to be relevant for optimization tasks. They are physically based, they capture the dominant phenomena and they can be implemented online. In backward modeling, the vehicle speed profile and the driver's torque demand are the main model inputs. The torque request at wheel, T^{sp}_{pwt}, depends on the driving conditions (speed and acceleration) and can be evaluated from drivers demand (throttle and brake pedal positions). Moreover:

$$T^{sp}_{pwt}(t) = R_1 T^{sp}_{mot,ss}(t) + R_{gb} T^{sp}_{eng,ss}(t) \quad (1)$$

where R_{gb} is the gear ratio and R_1 is the front axle ratio. The torque setpoint can be positive or negative depending on the vehicle operating conditions (traction or braking). $T^{sp}_{mot,ss}$ is the requested electric motor torque and the engine torque is the control input:

$$u(t) = T^{sp}_{eng,ss}(t) \quad (2)$$

The electric motor power, P_{elec}, is usually described by a map as a function of the motor torque and speed N_{mot}:

$$P_{elec}(t) = f_{elec}(T^{sp}_{mot,ss}, N_{mot}) \quad (3)$$

The engine Fuel Consumption (FC) and the NO_x emissions are provided by steady state maps that depend on the engine torque and speed N_e:

$$\dot{m}_f(t) = f_{FC}(T^{sp}_{eng,ss}, N_e) \quad (4)$$

$$\dot{m}_{NO_x}(t) = f_{NO_x}(T^{sp}_{eng,ss}, N_e) \quad (5)$$

These two maps describe the quasi-static performances resulting from the engine calibration. They will be introduced in the energy management strategy.

The fuel mass injected $\dot{m}_f$ is transformed into a fuel power using the lower heating value of the fuel Q_{lhv} which is a constant for a given fuel:

$$P_{fuel}(t) = Q_{lhv}\dot{m}_f(t) \quad (6)$$

The battery pack is modeled as a basic equivalent circuit comprising a voltage source U_0 placed in series with a resistance R_0. These two variables vary according to the battery State of Charge (SOC). The battery current and voltage are given by:

$$U_{bat} = U_0(SOC) - R_0(SOC) I_{bat} \quad (7)$$

$$I_{bat} = \frac{U_0}{2R_0} - \sqrt{\frac{U_0^2}{4R_0^2} - \frac{P_{elec}}{R_0}} \quad (8)$$

where the battery power is $P_{bat} = P_{elec} = U_{bat} I_{bat}$. The variation of battery SOC is computed from the battery current and power:

$$\dot{SOC}(t) = \begin{cases} -\dfrac{I_{bat}}{Q_0}, & \text{if } P_{elec} > 0 \\ -\eta_{bat}(SOC)\dfrac{I_{bat}}{Q_0}, & \text{else} \end{cases} \quad (9)$$

where Q_0 is the battery capacity and η_{bat} represents its Faradic efficiency. In the next section, the battery SOC

is the system state ($x(t) = SOC(t)$). The electrochemical battery power is:

$$P_{ec} = -Q_0 U_0(SOC)\dot{SOC}(t) \tag{10}$$

1.3 Supervisory Control Strategy

For hybrid electric vehicle, the total power delivered to the wheels comes from two energy sources: the fuel and a battery. The energy management strategy computes the best power split between these two sources. The proposed strategy is based on the ECMS previously developed [10-12] and is already implemented on a gasoline hybrid electric vehicle [1, 13]. In previous studies considering SI engines, the main optimization criterion was the overall fuel consumption. Thus, the problem formulation was to determine the command $u(t)$ that minimizes the cost function expressed as:

$$J = \int_{t_0}^{t_f} P_{fuel}(u,t)dt \tag{11}$$

For a Diesel HEV, this objective is modified and we chose to minimize a compromise between fuel consumption and NO_x emission. Then, the integral cost of the fuel is defined to be the integral of the weighted sum of the fuel consumption and the NO_x emission over the driving cycle. The idea is to merge the fuel map and the NO_x map in order to replace the fuel consumption-based cost by a weighted average of NO_x and fuel consumption. Thus, the fuel power defined by Equation (6) becomes:

$$P^*_{fuel} = Q_{lhv}\left[(1 - k_{fc/NO_x})\dot{m}_f + k_{fc/NO_x}\dot{m}_{NO_x}\right] \tag{12}$$

where the parameter k_{fc/NO_x} is used to set the trade-off between fuel consumption and NO_x emission. In order to ease the tuning of this parameter, the two maps must be comparable. Thus, the NO_x map is normalized such that its mean value remains close to the mean value of the fuel maps. The fuel mass flow rate and the NO_x emission strongly depend on the engine operating condition. As a first approximation, we use two static maps depending on engine speed and torque (*Eq. 4, 5*) and the optimal control problem is then:

$$\min_{u\in\mathscr{U}} \int_{t_0}^{t_f} P^*_{fuel}(u,t)dt \tag{13}$$

The state of the system is the State of Charge. Its dynamics writes:

$$\dot{x} = \alpha(x,u)\left(1 - \sqrt{1 - \beta(x)u}\right) \tag{14}$$

where α and β depend on the battery equivalent circuit characteristics (resistance R_0, voltage U_0, efficiency η_{bat}) and the SOC as described in Equations (7-9). The optimization problem has a state constraint such that the final value of the SOC $x(t_f)$ should be equal to its initial value $x(t_0)$. The system input is the engine torque request that belongs to an admissible space such that $\mathscr{U} = [T_{eng_{min}} T_{eng_{max}}]$. This optimization problem can be solved using the Pontryagin's Minimum Principle (PMP) where the optimal command writes:

$$u^{opt} = arg\min_{u\in\mathscr{U}} \mathscr{H}(x(t),\lambda(t),u(t),t) \tag{15}$$

where the Hamiltonian function is defined as:

$$\begin{aligned}\mathscr{H}(x(t),\lambda(t),u(t),t) = &\left[(1 - k_{fc/NO_x})\dot{m}_f(u,t)\right.\\ &\left. + k_{fc/NO_x}\dot{m}_{NO_x}(u,t)\right]\\ &- \lambda(t)\alpha(x,u)\left(1 - \sqrt{1 - \beta(x)u}\right)\end{aligned} \tag{16}$$

In first approximation, if U_0 and R_0 are constant (the *SOC* does not vary so much), the Hamiltonian can be rewritten as:

$$\mathscr{H}(x(t),\lambda(t),u(t),t) = P^*_{fuel}(t) + sP_{ec}(t) \tag{17}$$

The equivalence factor s weighs the electrochemical power. Its value modifies the balance between the electrochemical power use and the equivalent fuel power use. The equivalence factor is chosen such that the constraint on the final SOC is fulfilled $x(t_f) = x(t_0)$. In this paper, we assume the drive cycle is known and, under this assumption, the equivalence factor is a constant determined off-line. The sensitivity of this parameter and the online adaptation rule was studied by Chasse *et al.* for a SI engine in [13]. The robustness of this energy management for a Diesel HEV was studied by Thibault and Leroy in [14]. The method to determine the equivalence factor off-line according is described in [15]. In the next section, we present the influence of the weight between the fuel consumption and the NO_x emissions.

1.4 Results

The simulation results are presented in Figure 3. These simulations are performed from the fuel economy optimization to the NO_x abatement optimization. The weighting parameter k_{fc/NO_x} ranging from 0 (minimum of fuel consumption) to 1 (minimum of NO_x emission). The trends are clear for all the driving cycles considered (FTP, WLTP and ARTEMIS Urban): the weighting

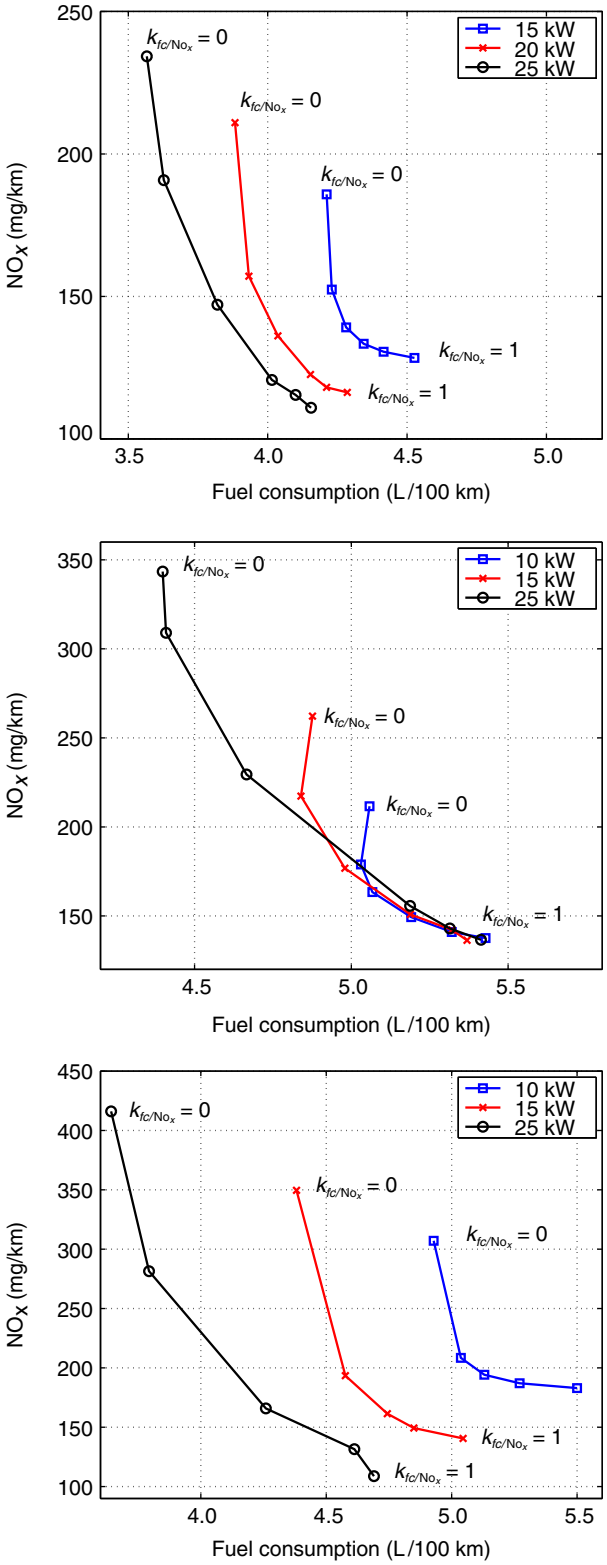

Figure 3

Evolution of the tradeoff betweeen NO_x emissions and fuel consumption for a parametric variation of the electric machine power and the weighting parameter k_{fc/NO_x}. From top to bottom: FTP, WLTP and ARTEMIS Urban.

parameter set the trade-off between FV and NO_x emission. For a pure NO_x optimisation, the Fuel Consumption (FC) penalty can be very high. However a fine tuning of k_{fc/NO_x} provides a great potential for limiting NO_x emission at a price of a very small increase of fuel consumption. The achievable NO_x reduction is close to 40% for FTP. On the other hand, the fuel penalty is small and does not exceed 5%. This behaviour can be observed for several values of the electric machine power.

Figure 4 shows the instantaneous values of some powertrain quantities during the experimental tests. The comparison concerns the HEV with a 20 kW electric motor. Two cases are presented: the fuel-economy optimization and the NO_x reduction optimization. The test results are summarized in Table 2 and in Figure 5. For the optimization of the fuel consumption, the electric motor is mostly used for traction during the urban part of the cycle while the Diesel engine is mostly used at high loads during the extra-urban part to recharge the battery. The ECMS allows to run the ICE mostly for high efficiency setpoints. For the NO_x reduction case, the instantaneous values of torque are limited and the optimal NO_x strategy avoids the high torque values (especially during the extra-urban part of the drive cycle). When the NO_x emissions are not considered ($k_{fc/NO_x} = 0$), the Diesel engine operates mostly at high loads where the engine efficiency is high. The selected operating points are close to the border limit of the LTC region where the amount of EGR is reduced compared to the NO_x optimal region. For the NO_x optimization case ($k_{fc/NO_x} = 0.5$), most of the selected operating conditions are located at middle engine loads. This region of the engine mapping represents a good compromise between NO_x emissions and fuel consumption. The pure engine mode or the recharging mode is limited to the middle torque operating conditions. These results prove that the adapted ECMS is suitable for the Diesel HEV and the optimal behavior is modified compared to the optimization policy applied for gasoline HEV.

2 TRANSIENT TORQUE CONTROL

2.1 Analysis of the Transient NO_x Emisssions

The pollutant emission behaviour of an engine is not purely quasi-static. Thus, the assumption that the emissions can be modeled using static maps can be inadequate. An example of transient NO_x emissions for a portion of a NEDC is displayed in Figure 6. This test was performed on a high dynamic test bench and the NO_x emissions were recorded with a gas analyzer.

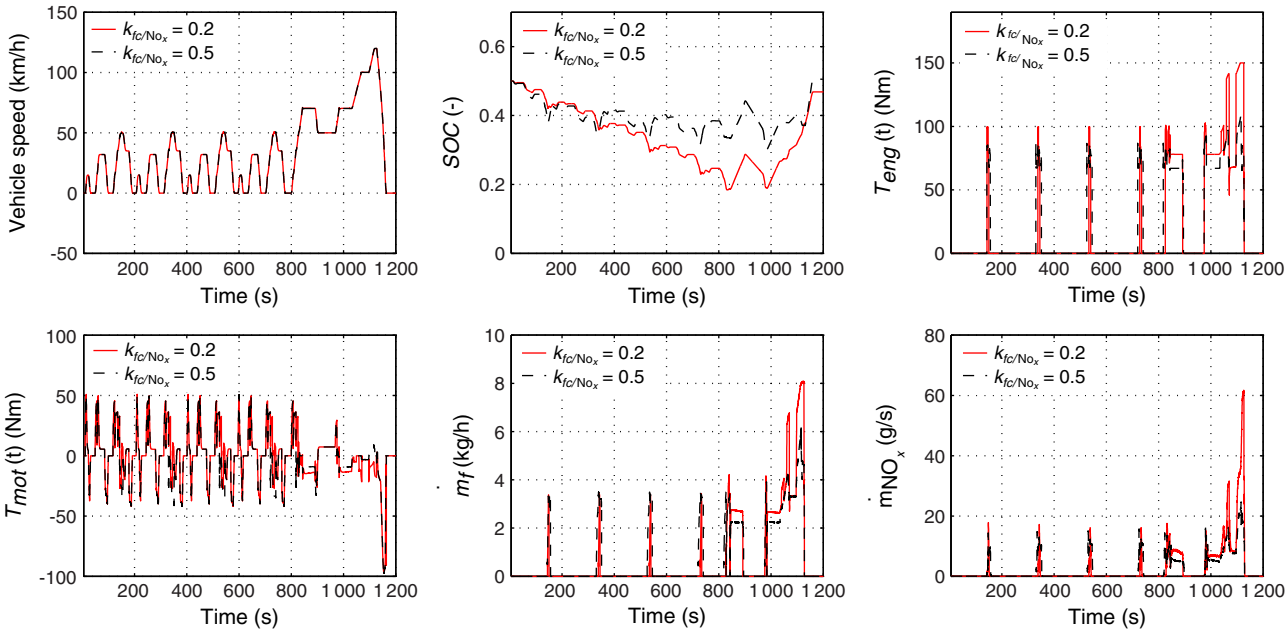

Figure 4

Experimental results for NEDC with the HEV with a 20 kW electric motor. Comparison of two optimisation trade-offs: fuel consumption oriented optimisation with $k_{fc/NO_x} = 0.2$ (red line) and NO_x-oriented optimisation with $k_{fc/NO_x} = 0.5$ (black dotted line).

TABLE 2

Experimental results for a NEDC: comparison of powertrain configuration including FC and NO_x oriented optimization

Vehicle	Baseline	S&S	HEV	HEV
EM power (kW)	-	-	20	20
Mass (kg)	1 470	1 470	1 630	1 630
k_{fc/NO_x}	-	-	0.2	0.5
FC (L/100 km)	4.5	4.16	3.43	3.5
NO_x (mg/km)	110	100	82	67
HC (mg/km)	120	111	20	27

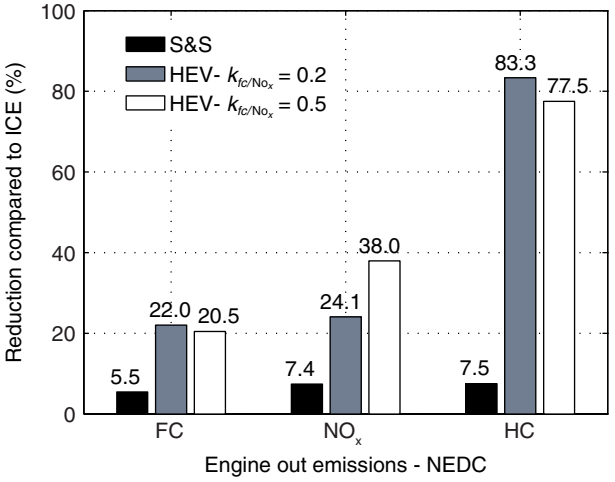

Figure 5

Summary of the experimental results. The gains are relatives to the stand-alone Diesel engine. Three configurations are displayed: Stop and Start, HEV with $k_{fc/NO_x} = 0.2$ and HEV with $k_{fc/NO_x} = 0.5$.

Figure 5 exhibits several peaks in NO_x during the first acceleration of the extra-urban part of the driving cycle. At each gear change, the injection cut-off decreases the exhaust equivalence ratio. This limits the availability of burned gas at the engine intake. During the transient, the intake Burned Gas Ratio (BGR) drops dramatically. When the driver re-accelerates, the intake BGR target cannot be reached instantaneously due to burned gas transport from the exhaust to the intake plenum. During this transient, the intake gas composition and thus the cylinder burned gas ratio are not in steady-state operating conditions leading to spikes in measured NO_x.

The transient part of the pollutant emission may vary according to the engine, its calibration and the driving cycle considered. In the experimental data presented in Figure 5, the instantaneous NO_x levels can be twice the

TABLE 3

Engine performances measured during NEDC and FTP driving cycles. The Transient Part (TP) contribution (in %) of the FC (in L/100 km) and NO_x (in mg/km) emissions are computed from the experimental measures and the engine static maps

	Driving cycle					
	NEDC			FTP		
	Bench	Map	TP	Bench	Map	TP
NO_x	110	100	9%	170	100	42%
FC	4.5	4.3	3%	4.7	4.4	6%

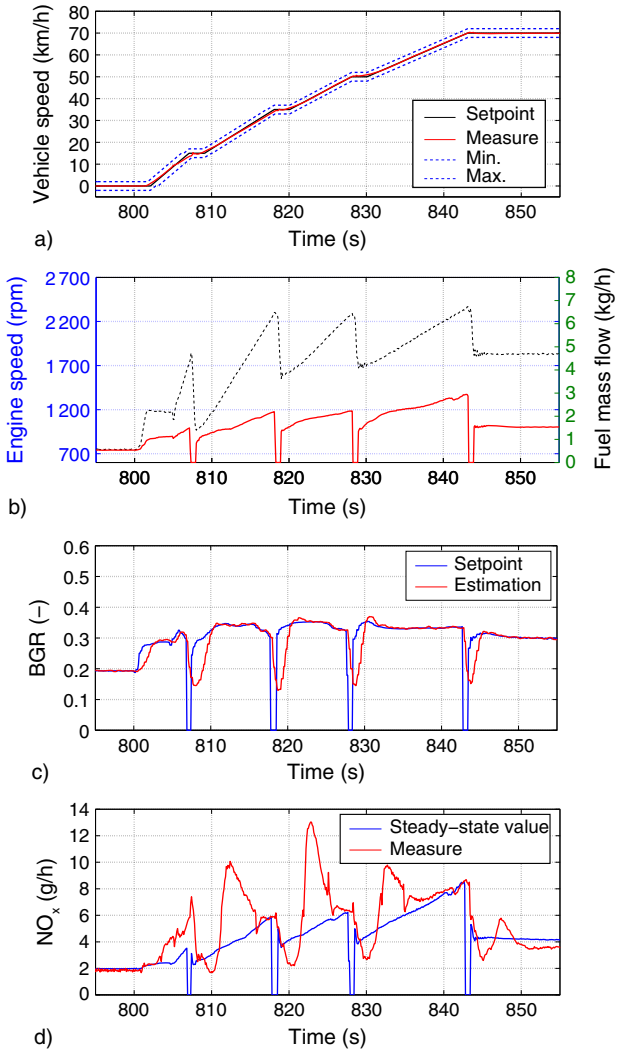

Figure 6

First acceleration of the extra-urban part of the NEDC. a) Vehicle speed, b) engine speed (dotted line) and fuel mass flow, c) BGR and d) NO_x emissions. The steady state NO_x value is calculated from a static map depending on engine speed and torque. The measured NO_x value is delayed and filtered due to the gas analyzer dynamics.

steady state values during transients. Table 3 recaps the transient NO_x contribution on the engine performances during driving cycles. These results correspond to a NECD and a FTP driving cycles performed in conventional engine-driven operations. For the NEDC, the transient NO_x contribution is lower than 9%. However, for the FTP cycle, the transient contribution rises up to 42%.

For the next generation Euro 7 vehicles, a new driving cycle (WLTC) is going to be defined. This latter is more representative of real driving conditions (such as the FTP) and imposes more drastic transient solicitations compared to the actual NEDC. Thus, a higher transient part of the total NO_x emissions is expected. This paper addresses this issue and aims at developing a suitable control strategy for Diesel HEV.

2.2 Transient Torque Control

NO_x peaks occurring during engine transients account for an important part of the total NO_x emissions. The reduction of the transient part of NO_x can be achieved by further improvements of the air system architecture (shorter LP EGR system, combination of HP and LP EGR systems, internal EGR using Variable Valve Actuation (VVA)) or by including a combustion control strategy to adapt injection settings according to air system errors (as proposed by [16]). Here, we consider a Diesel engine with a LP EGR system and without transient combustion control strategy. The goal is to take the advantage of the additional degree of freedom provided by the hybridization only. The idea is to use the electric machine to limit the internal combustion engine dynamics. Some preliminary solutions of transient emission limitation by means of electric boost are proposed in the literature. The limitation of the transient NO_x emissions by an adaptation of the transient torque demand is proposed by [17]. A similar approach, called

phlegmatising, was developed by [18]. Recently, Nuësch *et al.* [19] investigate the influence of considering transient emissions in Diesel hybrid electric vehicles. They consider nitrogen oxide and particulate matter using empirical emissions models.

2.2.1 Key Idea and Principle of the Strategy

Figure 7 shows the influence of the torque demand on the amplitude of a NO_x peak obtained with our experimental setup. The NO_x peak amplitude is higher for fast torque transient and these peaks decrease as far as the torque gradient decreases. Also, the NO_x peaks are well correlated with the BGR error ($\varepsilon F_1 = F_1^{sp} - F_1^{est}$). This figure demonstrates that the NO_x emissions are strongly linked with the torque demand and the amplitude of the peak increases with the torque gradient.

These results confirm the conclusion drawn by [17] and [18] who proposed heuristic methods consisting in a limitation of the engine torque setpoint dynamics. In this paper, we apply a similar principle while introducing models of the system to compute the limited engine torque demand. The principle of this strategy is illustrated in Figure 8.

The transient consists in an increasing engine torque step from point A to point B. In this case, the EMS proposes a torque step noted $T^{sp}_{eng,ss}$. This choice is the solution of Equation (15) (respecting (1)) computed from purely static maps without any consideration for the Diesel engine constraints. The principle of the strategy is to keep the same torque setpoint B requested by the EMS but the trajectory followed to reach this value is adapted. The torque setpoint control consists in defining a new torque trajectory $T^{sp}_{eng,t}$ from point A to point B′ (in red in *Fig. 8*) such that the transient NO_x peak is avoided or reduced. The torque request at wheel, T^{sp}_{pwt}, depends on the driving conditions (speed and acceleration) and can be evaluated from driver's demand (throttle and brake pedal positions). This demand can be satisfied using the engine, the electric motor or any combination of these two torque sources:

$$T^{sp}_{pwt}(t) = R_1 T^{sp}_{mot,ss}(t) + R_{gb} T^{sp}_{eng,ss}(t) \tag{18}$$

where R_{gb} is the gear ratio and R_1 is the front axle ratio. The torque setpoint can be positive or negative depending on the vehicle operating conditions (traction or braking). $T^{sp}_{mot,ss}$ is the electric motor torque setpoint and $T^{sp}_{eng,ss}$ is the engine torque setpoint. The steady-state split ratio is chosen by the EMS and the principle of the strategy is to modify its value during the engine transients only. In steady-state, the torque split ratio is maintained. In transient, Equation (18) is not modified but the steady-state engine and motor torques become two trajectories:

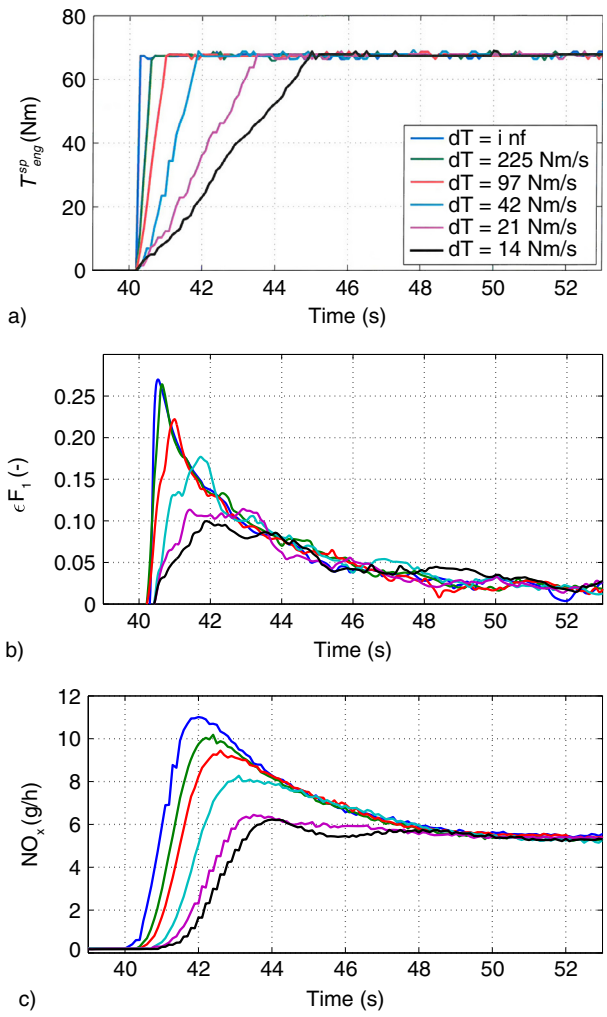

Figure 7

Experimental results of a transient representing an engine cut-off followed by a tip-in with a torque gradient limitation. a) Engine torque, b) BGR error and c) NO_x emissions.

$$T^{sp}_{pwt}(t) = R_1 T^{sp}_{mot,t}(t) + R_{gb} T^{sp}_{eng,t}(t) \tag{19}$$

In both cases, the torque request at wheel is not modified. The command $u(t)$ is defined as the motor torque correction $u(t) = \Delta T_{mot}$. Then, the dynamic motor torque request corresponding to the corrected motor torque setpoint is:

$$T^{sp}_{mot,t}(t) = T^{sp}_{mot,ss}(t) + u(t) \tag{20}$$

The command $u(t)$ is a portion of the motor torque that compensates for the engine torque during transients.

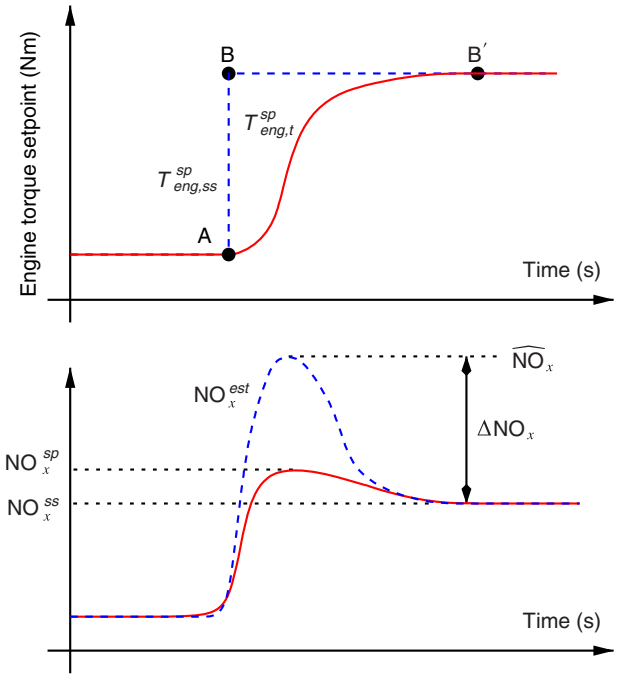

Figure 8

Principle of the control strategy to limit the amplitude of the NO_x peak during a torque step.

The command u is deduced from Equation (19) and (20) and it writes:

$$u(t) = \frac{T^{sp}_{pwt}(t) - R_{gb}T^{sp}_{eng,t}(t)}{R_1} - T^{sp}_{mot,ss}(t) \qquad (21)$$

The command $u(t)$ is directly linked to the static motor and powertrain torque setpoints and the dynamic torque setpoint $T^{sp}_{eng,t}$. This latter is a key variable and it is computed such that the NO_x peak generated during a transient is limited. The computation of the corrected engine torque demand $T^{sp}_{eng,t}$ (or trajectory) is explained in the next section. Following this approach, this strategy is applied in cascade with the EMS displayed in Figure 1. The ECMS determines the optimal operating points at some (relatively large) time scale, while a faster controller determines the engine and motor trajectories that minimize the NO_x emissions.

2.2.2 NO_x Modeling

Nitrogen oxides produced by Diesel engines mainly consist of Nitric Oxides (NO) and, to a lesser extent, of nitrogen dioxides (NO_x). In standard Diesel combustion conditions, NO is essentially produced by the extended Zeldovich mechanism. According to [20], under the equilibrium assumption, the initial NO_x formation rate (in $mol.cm^{-3}.s^{-1}$) may be written:

$$\frac{d[NO]}{d\theta} = \frac{1}{6N_e}\frac{6\cdot 10^{16}}{\Theta_b^{\frac{1}{2}}}\exp\left(-\frac{69\ 090}{\Theta_b}\right)[O_2]_e^{\frac{1}{2}}[N_2]_e \qquad (22)$$

where θ represents the crank angle, N_e is the engine speed, Θ_b the temperature in the burned gases and $[X]_e$ refers to the equilibrium concentration of the species X. NO_x formation is thus promoted by high O_2 concentrations and elevated temperatures in the post-combustion gases. Moreover, [21] experimentally shows that the critical time period is when burned gas temperatures are at a maximum. The complexity level of the model employed in the present study to predict NO_x emissions has to be compatible with its integration in the transient torque control strategy, preventing the use of a crank angle resolved thermodynamical model. As the torque trajectory is determined *a priori*, the use of measured values as input variables of the model is also banned. A semi-physical mean value model proposed by [22], and inspired by NO_x kinetics, has been chosen to estimate NO_x emissions. A detailed analysis of this model is proposed by [23]. NO_x concentration in the output of the cylinders is expressed as a function of the engine speed N_e, the intake manifold burned gas ratio F_1 and the maximum value of in-cylinder temperature $\hat{\Theta}_{cyl}$, according to the following expression:

$$NO_x = \alpha_1\left(\frac{N_e}{\alpha_2}\right)^{\alpha_3}\left(\alpha_4\left(\hat{\Theta}_{cyl} - \alpha_5\right)\right)^{\alpha_6(1-\alpha_7 F_1)} \qquad (23)$$

The coefficients α_i are calibration parameters learnt on experimental data. The values obtained for the Diesel engine considered in this paper are given in Table 4. In this model, the temperature in the burned gases has been replaced by the maximum value of the mean temperature in the cylinder for sake of simplicity, as the temperature in the burned gases is not measurable for control applications. In spite of this simplification, the model predicts NO_x emissions with a good accuracy over the whole engine operating range as well as for variations of BGR, as shown in [23]. An example of the NO_x model sensitivity according to a BGR variation is displayed in Figure 9.

TABLE 4

NO_x model parameters

α_1	α_2	α_3	α_4	α_5	α_6	α_7
0.37	3 250	-0.56	12.4	0.63	3.06	1.15

MVM model validations in transient are reported in Figures 10 and 11.

During transients, the intake manifold gas compositions are not in steady-state operating conditions. The maximum in-cylinder temperature reaches its steady-state values much faster, and as a result, is considered to be quasi-static. A simplified model is used to represent the dynamics of the intake manifold burned gas ratio (*Eq. 24*). It consists of a delayed first order filter of the BGR static value:

$$\tau(t)\dot{F}_1^{est}(t) + F_1^{est}(t) = F_1^{ss}(t - t_d(t)) \tag{24}$$

where the time constant τ and the time delay t_d are parametrized as a function of the engine speed:

$$\tau(t) = \frac{\beta_f}{N_e(t)} \tag{25}$$

and

$$\tau_d(t) = \begin{cases} \frac{\beta_d}{N_e(t)}, & \text{if } T_{eng}^{sp}(t) > 0 \\ 0, & \text{else} \end{cases} \tag{26}$$

The BGR map F_1 has the general form:

$$F_1 = \vartheta(N_e, T_{eng}) \tag{27}$$

The burned gas ratio dynamic model is compared with experimental results in Figure 12. The model is in good agreement with the observed test data and can be used as a reference EGR system model into the torque control strategy.

Table 5 compares the estimated cumulated emissions and the NO_x transient contribution on these emissions during driving cycles with the corresponding experimental results given in Table 3. The model correctly predicts both the cumulated NO_x emissions and the transient part. It is employed to validate the NO_x limitation strategy in simulation.

2.2.3 Engine Torque Setpoint Correction

This section explains how to compute the corrected engine torque trajectory. The transient correction of

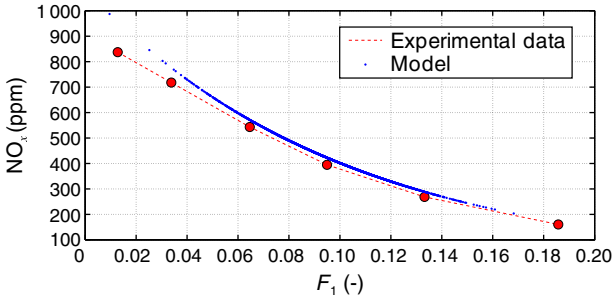

Figure 9

Comparison between the NO_x model and experimental data for a BGR variation.

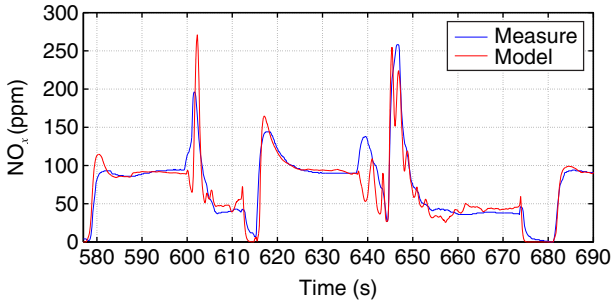

Figure 10

Comparison between NO_x model and experimental data for a portion of NEDC driving cycle.

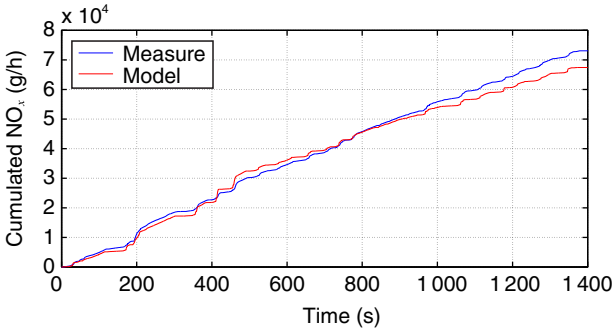

Figure 11

Comparison between the cumulated NO_x model and experimental data for a FTP driving cycle.

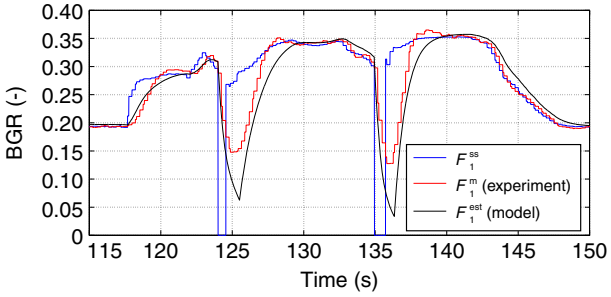

Figure 12

Comparison between measured and estimated intake manifold burned gas fraction (top) and NO_x emission (bottom) during a gear change.

TABLE 5

Comparison between measured and estimated NO_x emissions during NEDC and FTP driving cycle. The experimental Steady-State Part (SSP) of the emissions are computed from the static map. The estimated steady-state emissions are calculated from the model using the intake BGR setpoint F_1^{sp}

	Driving cycle					
	NEDC			FTP		
	Total (mg/km)	SSP (mg/km)	TP (%)	Total (mg/km)	SSP (mg/km)	TP (%)
Bench	110	100	9	170	100	42
Model	109	94	14	179	125	30

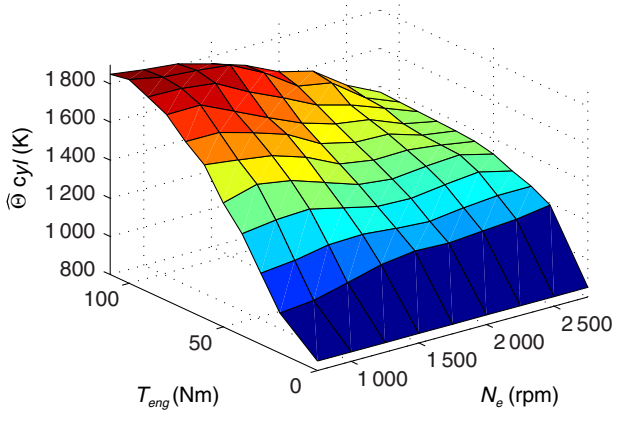

Figure 13

Maximum cylinder temperature map.

the torque setpoint requested by the EMS relies on a Mean Value Model (MVM) of the engine NO_x emissions presented in the previous subsection. This model links the NO_x emissions with the engine speed (N_e), the intake BGR (F_1) and the maximum cylinder temperature ($\hat{\Theta}_{cyl}$). These variables are recognized as first order variables of NO_x formation in compression-ignition engines. The NO_x model, has the general form:

$$NO_x = \phi(N_e, \hat{\Theta}_{cyl}, F_1) \tag{28}$$

The steady-state NO_x level is:

$$NO_x^{ss} = \phi(N_e, \hat{\Theta}_{cyl}^{ss}, F_1^{ss}) \tag{29}$$

The BGR sepoint F_1^{ss} is computed from a static map (27). Temperature setpoint, $\hat{\Theta}_{cyl}^{ss}$ is also mapped according to engine speed and torque (*Fig. 13*):

$$\begin{cases} F_1^{ss} & = \vartheta(N_e, T_{eng,ss}^{sp}) \\ \hat{\Theta}_{cyl}^{ss} & = \psi_1(N_e, T_{eng,ss}^{sp}) \end{cases} \tag{30}$$

During a transient, the BGR is not equal to its setpoint due to the EGR system lag (as displayed in *Fig. 6*). For the engine control, an online estimation of the BGR is used [24]. This estimation is valid for the actual BGR value, however, we need to determine the expected BGR value before the transient has occurred. Then, this estimation cannot be used for the high level torque control strategy. Here, the burned gas transport delay from exhaust manifold to intake manifold is modeled using the MVM detailed previously. This model provides the estimated BGR (F_1^{est}) assuming a first order dynamics and a pure delay applied to the BGR map as described in Equation (24). The function ϕ appearing in Equation (28) is invertible and a cylinder temperature setpoint can be computed from this BGR estimation and from the target NO_x^{sp} (*Fig. 8*):

$$\hat{\Theta}_{cyl}^{sp} = \phi^{-1}(N_e, NO_x^{sp}, F_1^{est}) \tag{31}$$

The NO_x target computation is explained in the next subsection. Knowing $\hat{\Theta}_{cyl}^{sp}$, the cylinder temperature map ψ_1 can be inverted in order to find the corrected value of the engine torque (or torque trajectory):

$$T_{eng}^{t} = \psi_1^{-1}(N_e, \hat{\Theta}_{cyl}^{sp}) \tag{32}$$

For sake of simplicity, we assume that the static maximum temperature map ψ_1, established for the nominal BGR setpoint, is representative of the actual BGR condition. A dependency of the temperature map according to the actual BGR would provide acceptable results. For that, the cylinder temperature map ψ_1 can be modified as follows:

$$\hat{\Theta}_{cyl} = \psi_2^{-1}(N_e, T_{eng}, F_1) \tag{33}$$

Adding this dependency into a modified function ψ_2 will increase the calibration part of the strategy. We are currently investigating a model-based approach to reduce the experimental tests needed for the calibration

of the maximum temperature function ψ_2. This work is not the purpose of this paper and will be reported in a further paper with the justification for the BGR dependency simplification in map ψ_1.

2.2.4 NO_x Target Definition

This section explains how to compute the NO_x trajectory used for torque trajectory computation. The NO_x target definition is purely heuristic and relies on a tunable reduction factor of the maximum NO_x peak amplitude. The achievable NO_x target NO_x^{sp} (*Fig. 8*) is supposed to be included between the actual (or estimated) value and the steady-state value:

$$NO_x^{est} \geq NO_x^{sp} \geq NO_x^{ss} \tag{34}$$

The target NO_x is tuned empirically with a reduction factor ξ such that:

$$NO_x^{sp} = NO_x^{ss} + \Delta NO_x\left(1 - \frac{\xi}{100}\right) \tag{35}$$

where ΔNO_x is the amplitude of the NO_x peak referred as the steady NO_x value as shown in Figure 8:

$$\Delta NO_x = \widehat{NO}_x - NO_x^{ss} \tag{36}$$

This method is simple and allows to flexibly tune the level of NO_x reduction. However, the ability for the system to achieve this target is not guaranteed because the system saturation is not considered. Moreover, the reduction factor ξ value is constant for each transient. Including the system saturation to define what can be the reachable NO_x target is a necessary improvement to make the transient torque controller more generic and easy to tune. This will lead to define a limiting factor ξ according to a feasible NO_x target instead of an empirical one. This is the main perspective of this work.

2.2.5 Actuator Limitation and System Saturation

The torque control strategy must account for the actuator limitation that depends on the maximum motor torque T_{mot}^{max} and the static motor torque defined by:

$$T_{mot,ss}^{sp}(t) = \frac{T_{pwt}^{sp}(t) - R_{gb}T_{eng,ss}^{sp}(t)}{R_1} \tag{37}$$

Then the command $u(t)$ is bounded such that:

$$u(t) \in \left[0(T_{mot}^{max} - T_{mot,ss}^{sp}(t))\right] \tag{38}$$

From Equations (21, 37) and (38), the minimum and maximum engine torque values write:

$$\begin{cases} T_{eng}^{sp,min} & = \frac{T_{pwt}^{sp} - R_1 T_{mot}^{max}}{R_{gb}} \\ T_{eng}^{sp,max} & = T_{eng,ss}^{sp} \end{cases} \tag{39}$$

The transient engine torque setpoint is obtained by saturating the engine torque trajectory (32):

$$T_{eng,t}^{sp} = sat\left(\min(T_{eng}^{t}, T_{eng}^{f}), T_{eng}^{sp,min}, T_{eng}^{sp,max}\right) \tag{40}$$

The notation $sat(u, u_m, u_M)$ is used for the function defined by:

$$sat(u, u_m, u_M) = \begin{cases} u_{min} & \text{if} \quad u(t) \leq u_m \\ u & \text{if} \quad u_m \leq u(t) \leq u_M \\ u_{max} & \text{if} \quad u_M \leq u(t) \end{cases} \tag{41}$$

T_{eng}^{f} is the feasible torque trajectory that defines the achievable transient NO_x emissions. This latter corresponds to the existing minimum value of the NO_x emissions that can be performed during transient conditions where the cylinder oxygen content (*i.e.* BGR) is not in steady-state condition. The system saturation is not included in this paper and is an ongoing work at IFP Energies nouvelles. Thus, the transient engine torque setpoint writes:

$$T_{eng,t}^{sp} = sat\left(T_{eng}^{t}, T_{eng}^{sp,min}, T_{eng}^{sp,max}\right) \tag{42}$$

2.3 Results

This section presents the simulation results of the transient torque control strategy. The objective is to determine whether limiting the Transient Part (TP) of the total NO_x emissions is possible or not. We also would like to characterize the influence of the strategy on the Steady-State Part (SSP) of the total NO_x emissions as well as the Fuel Consumption (FC).

A simulation platform modelling the complete hybrid vehicle has been developed to simulate driving cycles. In this paper, we consider the FTP. The idea is to simulate the system for several values of the NO_x reduction factor ξ ranging from 0% (baseline case) to 100%. This latter case corresponds to a limitation of all the NO_x emissions TP. In order to compare these simulations, the equivalence factor is adapted (dotted line in *Fig. 1*). The value of the equivalence factor was found by dichotomy in order to satisfy the constraint on the final battery state of charge:

$$SOC(t_0) = SOC(t_f) = 50\% \tag{43}$$

t_0 and t_f are the initial and final times of the considered driving cycle. The simulations are made for three hybridization levels defined by the power of the electric motor:

$$P_{mot} = \{8 \text{ kW}; 14 \text{ kW}; 20 \text{ kW}\} \quad (44)$$

To be realistic, the battery capacity and vehicle mass are adapted to the electric motor power as described in [15]. Pure electric driving is only enabled in the 20 kW case. The EMS finds the steady-state optimal torque split repartition which minimizes a trade-off between quasi-static NO_x and fuel consumption. The results displayed are obtained for a constant value of the parameter $k_{fc/NO_x} = 0.4$ in Equation (15). The impact of the hybridization level and this setting variable on NO_x emissions and fuel consumption for a Diesel HEV is not the purpose of this paper since it affects only the static balance between NO_x and FC. A sensitivity analysis was done by [25].

The strategy acts on transient phases involving increasing BGR setpoint. Figure 14 illustrates its action on two torque transients belonging to the FTP (*Fig. 15*). $\xi = 0\%$ corresponds to the reference case, without transient strategy; the two others cases (50% and 90%) illustrate the impact of the adjustable transient NO_x reduction parameter. For the second torque transient ($t = 203$ s), the NO_x peak can be completely avoided and the tuning parameter allows a flexible reduction of the peak's amplitude. This reduction is made by limiting the maximal cylinder temperature until enough burned gas is available. In the first torque transient ($t = 199$ s), a saturation on NO_x reduction is observed between the 50% and 90% cases. This saturation can be easily explained looking at the motor torque setpoint which has already reached its maximal value (T_{mot}^{max}) for $\xi = 50\%$. As a consequence, NO_x abatement is not achievable without increasing the electric motor maximum torque (*i.e.* the motor size). We can notice that the strategy does not affect the steady-state engine and motor torque setpoints as claimed in the previous section. They are equal to the one chosen by the EMS once the transient is over ($T_{mot,ss}^{sp} = T_{mot,t}^{sp}$ and $T_{eng,ss}^{sp} = T_{eng,t}^{sp}$).

The impact of the transient strategy on the battery SOC during a complete FTP is illustrated in Figure 16. When the strategy is enabled, the SOC decreases progressively because of the electric energy spent to cut NO_x peaks during each transient phase. The missing energy must be recuperated in order to complete the driving cycle with a final SOC constraint respected. This was done by adjusting the equivalence factor in the energy management strategy which slightly modifies the static operating point choice.

The effect of the strategy on the cumulated NO_x emissions and fuel consumption is illustrated in Figure 17.

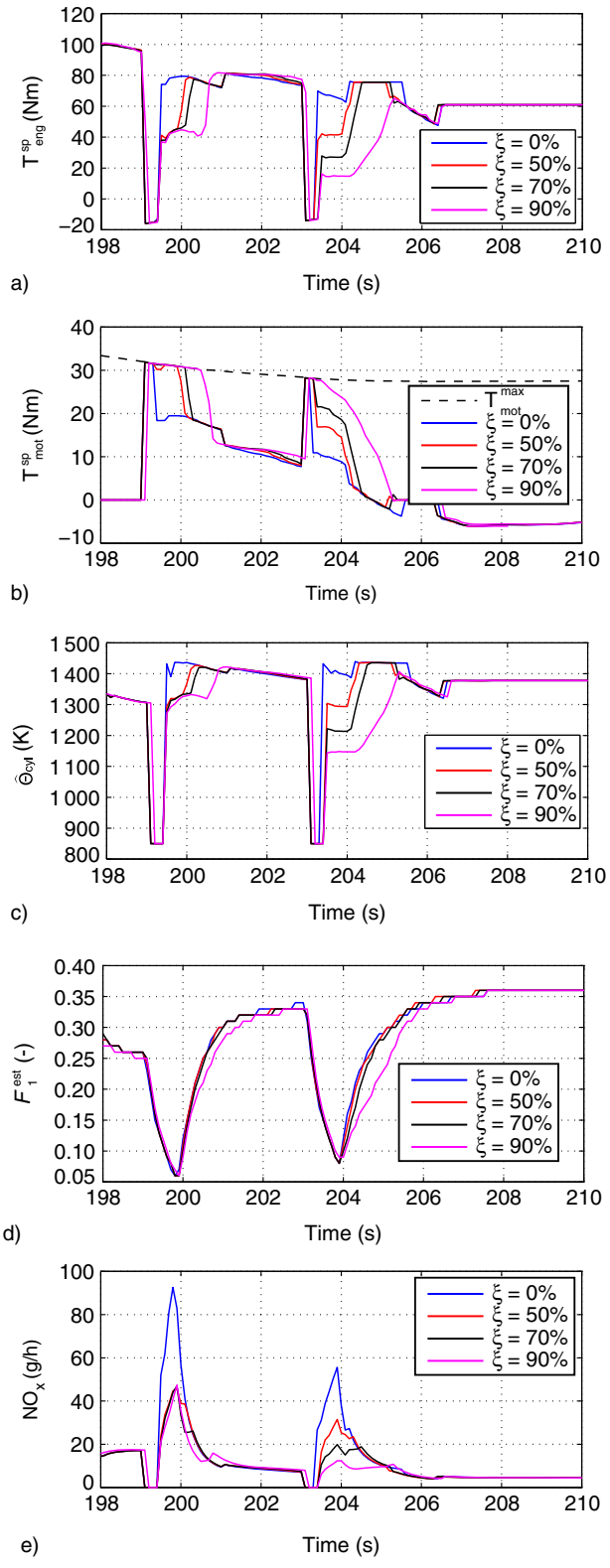

Figure 14

Impact of the transient strategy parameter ξ – FTP Full Hybrid 20 kW. a) Engine torque, b) motor torque, c) maximal cylinder temperature, d) burned gas ratio and e) NO_x emissions.

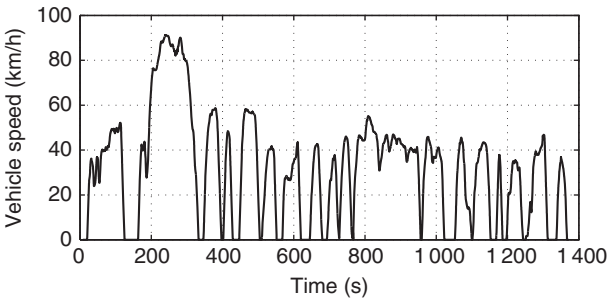

Figure 15

FTP vehicle speed profile.

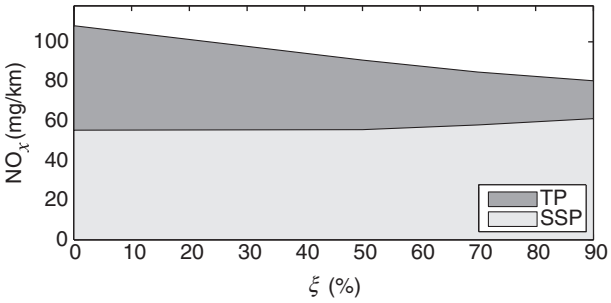

Figure 18

Impact of the transient strategy parameter ξ on the NO_x transient part – FTP Full Hybrid 20 kW.

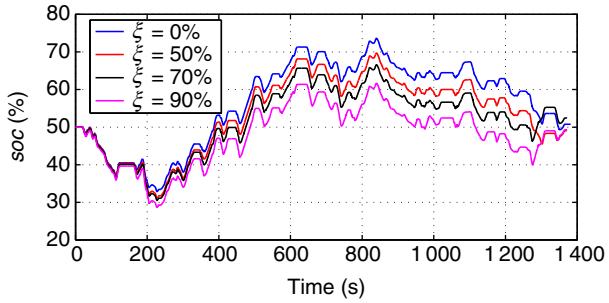

Figure 16

Impact of the transient strategy on the battery SOC – FTP Full Hybrid 20 kW.

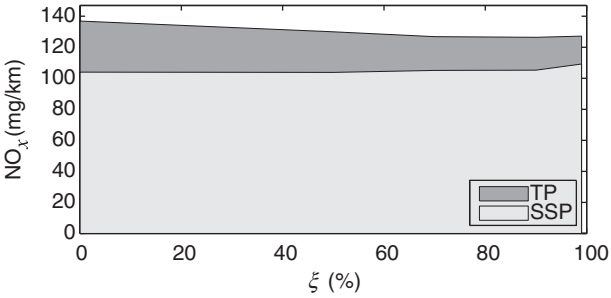

Figure 19

Impact of the transient strategy parameter ξ on the NO_x transient part – FTP Mild Hybrid 14 kW.

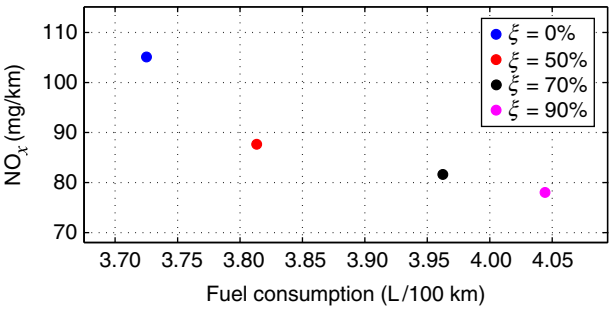

Figure 17

Impact of the transient strategy parameter ξ on the trade-off between NO_x emissions and fuel consumption – FTP Full Hybrid 20 kW.

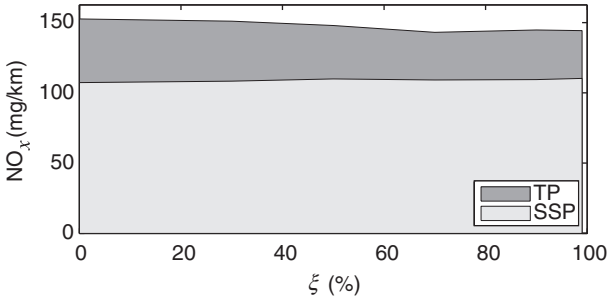

Figure 20

Impact of the transient strategy parameter ξ on the NO_x transient part – FTP Mild Hybrid 8 kW.

Due to transient peak reduction, the total NO_x emissions significantly drop at the price of a slight increase of fuel consumption. This demonstrates the interest of choosing a partial NO_x reduction instead of a total elimination. Indeed in this case, the most interesting case is $\xi = 50\%$ since it allows a global NO_x reduction of 17% with a fuel penalty of only 2%.

The transient part of NO_x emissions can be controlled with the damping factor ξ as illustrated in Figures 18, 19 and 20. The TP of NO_x emissions is defined as the

difference between total and steady-state emissions. The total emissions are computed from the model (28):

$$NO_x^{est} = \phi(N_e, \psi_1(N_e, T_{eng,t}^{sp}), F_1^{est}) \quad (45)$$

The steady-state NO_x emissions are computed with the same NO_x model. But, instead of using the estimated BGR as input, we use its steady-state value computed from the map (27):

$$NO_x^{ss} = \phi(N_e, \psi_1(N_e, T_{eng,t}^{sp}), \vartheta(N_e, T_{eng,t}^{sp})) \quad (46)$$

They represent what the emissions would be if the exhaust gas recirculation loop had an instantaneous settling time. Even if the static part of the cumulated NO_x emissions increases slightly with ξ due to the slight modification of static operating points, the total NO_x emissions are decreasing. The strategy allows to divide the transient part by two (from 49% to 24%) while the cumulated NO_x emissions are reduced by 26%. For $\xi = 90\%$, the remaining transient part corresponds to the saturation of the electric motor which is not able to provide enough torque.

For lower hybridization levels (14 kW and 8 kW), the electric torque available to allow transient NO_x reduction is lower and the emissions can not be reduced as much as in the full hybrid case. In the 8 kW, the electric motor saturation is quickly reached. As a consequence the transient NO_x is limited (*Fig. 20*).

As a conclusion, the transient strategy allows to control the NO_x transient emissions as long as the maximal electric motor torque is not reached. With a 20 kW electric motor, a spectacular NO_x reduction is achievable with a reasonable increase in fuel consumption. The value of the damping factor ξ tunes the trade-off between the NO_x TP and the FC.

CONCLUSION

In Diesel hybrid vehicles, steady-state and transient NO_x emissions must be considered in the supervision strategy. First, we adapted the ECMS-based energy management strategy to account for the steady NO_x . An additional tuning parameter was introduced into the ECMS and allows to tune the trade-off between NO_x abatement and fuel consumption reduction. These results clearly demonstrate that model-based strategy (ECMS) allows an easy integration of the NO_x objective. In addition to the simulation results, the adapted ECMS is validated on the experimental hybrid test bench. The trend observed using the simulator was experimentally reproduced leading to a substantial reduction of the NO_x emissions. In addition, we introduced a torque control cascaded with the EMS in order to correct the torque split ratio computed by the ECMS. This strategy focuses on transient NO_x emissions and adapts the torque split ratio during transient operations where NO_x peaks are produced. The strategy tends to smooth the engine torque using the motor torque as torque compensator. This controller uses a mean value model for the intake manifold burned gas ratio dynamics and for the NO_x production. Using such models into a vehicle supervision level is the novelty of the approach. The simulation results have shown that the transient part of the NO_x emissions can be reduced. The strategy allows to limit the transient part of the emissions without modifying the steady-state part. Also, the use of the electric motor during transients has a price and the transient NO_x reduction slightly increases fuel consumption. This trade-off can be tuned with the reduction factor. The proposed strategy can be valuable to deal with driving cycles presenting more transient phases. This will be the case for Euro 7 vehicles with the new worldwide harmonized light-duty transient cycle.

REFERENCES

1 Chasse A., Chauvin J., Sciarretta A. (2010) Online optimal control of a parallel hybrid with costate adaptation rule, *Proceedings of the 6th IFAC Symposium Advances in Automotive Control*, Munich, 12-14 July. pp. 318-331.

2 Johnson V.H., Wipke K.B., Rausen D.J. (2009) HEV control strategy for real-time, *SAE Technical Paper* 2009-24-0068.

3 Montazeri-Gh M., Poursamad A., Ghalichi B. (2006) Application of genetic algorithm for optimization of control strategy in parallel hybrid electric vehicles, *Journal of the Franklin Institute* **343**, 4-5, 420-435.

4 Lin C.-C., Peng H., Grizzle J.W., Kang J.-M. (2003) Power management strategy for a parallel hybrid electric truck, *IEEE Transactions on Control Systems Technology* **11**, 6, 839-849.

5 Musardo C., Rizzoni G., Staccia B. (2005) A-ECMS: An adaptive algorithm for hybrid electric vehicle energy management, *Proceedings of the 44th IEEE Conference on Decision and Control*, Seville, 12-15 Dec.

6 Musardo C., Staccia B., Midlam-Mohler S., Guezennec Y., Rizzoni G. (2005) Supervisory control for NO*x* reduction of an HEV with a mixed-mode HCCI/CIDI engine, *Proceedings of the American Control Conference*, Portland, OR, 8-10 June.

7 Dextreit C., Kolmanovsky I.V. (2013) Game theory controller for hybrid electric vehicles, *IEEE Transactions on Control Systems Technology* **PP**, 99, 1-1.

8 Chasse A., Pognant-Gros P., Sciarretta A. (2009) Online implementation of an optimal supervisory control for a parallel hybrid powertrain, *SAE Paper* 2009–01-1868, *SAE Int. J. Engines* **2**, 1, 1630-1638.

9 Del Mastro A., Chasse A., Pognant-Gros P., Corde G., Perez F., Gallo F., Hennequet G. (2009) Advanced hybrid vehicle simulation: from "virtual" to "HyHiL" test bench, *SAE Technical Paper* 2009-24-0068.

10 Ambühl D., Sciarretta A., Onder C., Guzzella L., Sterzing S., Mann K., Kraft D., Küsell M. (2007) A causal operation strategy for hybrid electric vehicles based on optimal control theory, *Proceedings of the 4th Symposium on Hybrid Vehicles and Energy Management*, Stadthalle Braunschweig, Germany, Feb. pp. 318-331.

11 Sciarretta A., Guzzella L. (2007) Control of hybrid electric vehicles - optimal energy management strategies, *IEEE Control Systems Magazine* **27**, 2, 60-70.

12 Sciarretta A., Back M., Guzzella L. (2004) Optimal control of parallel hybrid electric vehicles, *IEEE Transactions on Control Systems Technology* **12**, 3, 352-363.

13 Chasse A., Hafidi G., Pognant-Gros P., Sciarretta A. (2009) Supervisory control of hybrid powertrains: an experimental benchmark of offline optimization and online energy management, *Proceedings of E-COSM'09 - IFAC Workshop on Engine and Powertrain Control, Simulation and Modeling*, Rueil-Malmaison, France, Dec.

14 Thibault L., Leroy T. (2013) Optimal online energy management for Diesel HEV: Robustness to real driving conditions, *SAE Technical Paper* 2013-01-1471.

15 Grondin O., Thibault L., Moulin P., Chasse A. (2011) Energy management strategy for Diesel hybrid electric vehicle, *Proceedings of the 7th IEEE Vehicle Power and Propulsion Conference (VPPC'11)*, Chicago, USA, 6-9 Sept.

16 Hillion M., Chauvin J., Petit N. (2011) Control of highly diluted combustion in Diesel engines, *Control Engineering Practice* **19**, 11, 1274-1286.

17 Predelli O., Bunar F., Manns J., Buchwald R., Sommer A. (2007) Laying out Diesel-engine control systems in passenger-car hybrid drives, *Proceeding of the 4th symposium on Hybrid Vehicle and Energy Management*, Stadthalle Braunschweig, Germany, 14-15 Feb. pp. 131-151.

18 Lindenkamp N., Stöber-Schmidt C.-P., Eilts P. (2009) Strategies for reducing NO*x* and particulate matter emissions in Diesel hybrid electric vehicles, *SAE Technical Paper* 2009-01-1305.

19 Nüesch T., Wang M., Voser C., Guzzella L (2012) Optimal energy management and sizing for hybrid electric vehicles considering transient emissions, *2012 IFAC Workshop on Engine and Powertrain Control Simulation and Modeling*, Rueil-Malmaison, France, 23-25 Oct.

20 Bowman C.T. (1975) Kinetics of pollutant formation and destruction in combustion, *Progress in Energy and Combustion Science* **1**, 1, 33-45.

21 Heywood J.B. (1988) *Internal Combustion Engine Fundamentals*, McGraw-Hill, New york.

22 Schmitt J.-C., Fremovici M., Grondin O., Le Berr F. (2009) Compression ignition engine model supporting powertrain development, *Proceeding of the E-COSM Symposium*, Rueil-Malmaison, France, 30 Nov. – 2 Dec. pp. 75-82.

23 Quérel C., Grondin O., Letellier C. (2012) State of the art and analysis of control oriented NOx models, *SAE Technical Paper* 2012-01-0723.

24 Grondin O., Moulin P., Chauvin J. (2009) Control of a turbocharged Diesel engine fitted with high pressure and low pressure exhaust gas recirculation system, *Proceedings of the 48th IEEE Conference on Decision and Control & Chinese Control Conference*, Shanghai, China, 16-18 Dec.

25 Thibault L., Grondin O., Quérel C., Corde G. (2012) Energy management strategy and optimal hybridization level for a Diesel HEV, *SAE Technical Paper* 201201-1019.

Manuscript accepted in December 2013
Published online in April 2014

Cite this article as: O. Grondin, L. Thibault and C. Quérel (2015). Energy Management Strategies for Diesel Hybrid Electric Vehicle, *Oil Gas Sci. Technol* **70**, 1, 125-141.